Astronomy
&
Astrophysics

Hydrogen Lyman-α and Lyman-β spectral radiance profiles in the quiet Sun

H. Tian[1,2], W. Curdt[1], E. Marsch[1], and U. Schühle[1]

[1] Max-Planck-Institut für Sonnensystemforschung, Max-Planck-Str. 2, 37191 Katlenburg-Lindau, Germany
e-mail: tianhui924@gmail.com
[2] School of Earth and Space Sciences, Peking University, PR China

ABSTRACT

Aims. We extend earlier work by studying the line profiles of the hydrogen Lyman-α and Lyman-β lines in the quiet Sun. They were obtained quasi-simultaneously in a raster scan with a size of about $150'' \times 120''$ near disk center.

Methods. The self-reversal depths of the Ly-α and Ly-β profiles. we are quantified by measuring the maximum spectral radiances of the two horns and the minimum spectral radiance of the central reversal. The information on the asymmetries of the Ly-α and Ly-β profiles is obtained through calculating the 1st and 3rd-order moments of the line profiles. By comparing maps of self-reversal depths and the moments with radiance images of the Lyman lines, photospheric magnetograms, and Dopplergrams of two other optically thin lines, we studied the spatial distribution of the Ly-α and Ly-β profiles with different self-reversal depths, and investigated the relationship between profile asymmetries and flows in the solar atmosphere.

Results. We find that the emissions of the Lyman lines tend to be more strongly absorbed in the internetwork, as compared to those in the network region. Almost all of the Ly-α profiles are self-reversed, while about 17% of the Ly-β profiles are not reversed. The ratio of Ly-α and Ly-β intensities seems to be independent of the magnetic field strength. Most Ly-α profiles are stronger in the blue horn, whereas most Ly-β profiles are stronger in the red horn. However, the opposite asymmetries of Ly-α and Ly-β are not correlated pixel-to-pixel. We also confirm that when larger transition-region downflows are present, the Ly-α and Ly-β profiles are more enhanced in the blue and red horns, respectively. The first-order moment of Ly-β, which reflects the combined effects of the profile asymmetry and motion of the emitting material, strongly correlates with the Doppler shifts of the Si III and O VI lines, while this correlation is much weaker for Ly-α. Our analysis shows that both Ly-α and Ly-β might be more redshifted if stronger transition-region downflows are present. We also find that the observed average Ly-β profile is redshifted with respect to its rest position.

1. Introduction

Hydrogen is the most abundant element in the solar atmosphere. And thus its resonance lines, especially the Lyman-alpha (Ly-α) and Lyman-beta (Ly-β) lines, play an important role in the overall radiative energy transport of the Sun (Fontenla et al. 1988).

Ly-α is by far the strongest line in the vacuum ultraviolet (VUV) spectral range. It is so dominant that $\approx 75\%$ of the integrated radiance from 800 Å to 1500 Å in the quiet Sun come from this single line (Wilhelm et al. 1998). Energy losses through the Ly-α emission are the most important radiative losses in the lower transition region, where the approximate temperature ranges from 8000 K to 30 000 K (Fontenla et al. 1988). Also, the spectral irradiance at the center of the solar Ly-α line profile is the main excitation source responsible for the atomic hydrogen resonant scattering in cool cometary and planetary material, and thus is required in modelling the Ly-α emissions occurring in cool interplanetary environments (Emerich et al. 2005).

About three decades ago, detailed observations of the Ly-α and Ly-β line profiles were performed with the NRL slit spectrometer onboard *Skylab* (e.g. Nicolas et al. 1976) and the UV polychromator onboard *OSO 8* (Orbiting Solar Observatory) (e.g. Lemaire et al. 1978; Vial 1982). Basri et al. (1979) used high-resolution Ly-α spectra obtained by the HRTS (High Resolution Telescope and Spectrograph) instrument on rocket

flight to investigate the network contrast and center-to-limb variation in the line profiles. Later, Ly-α profiles with both high spectral and spatial resolutions were obtained by the UVSP instrument onboard *SMM* (Solar Maximum Mission, e.g., Fontenla et al. 1988). The early studies on the Ly-α and Ly-β line profiles revealed clearly that the Lyman lines are highly variable not only in time, but also in space. However, these early observations were hampered by the strong geocoronal absorption at the line center.

The problem of geocoronal absorption went away, and high spectral, temporal, and spatial resolution observation of the Lyman lines could be obtained, when in 1995 the *SoHO* (Solar and Heliospheric observatory) space probe was positioned into an orbit around the first Lagrangian Point, L$_1$. The solar ultraviolet measurements of emitted radiation spectrograph (SUMER, Wilhelm et al. 1995; Lemaire et al. 1997) covers the whole hydrogen Lyman series as well as the Lyman continuum (Curdt et al. 2001), and provides full line profiles in high spatial and spectral resolution of 1″ and 44 mÅ, respectively. However, since the Ly-α line is so prominent, its high radiance leads to saturation of the detector microchannel plates. To overcome this shortcoming, 1:10 attenuating grids above 50 pixels on both sides of the detectors had been introduced into the optical design of the instrument (Wilhelm et al. 1995). But unfortunately, the attenuators also cause unpredictable modifications of the line profiles. By using SUMER data, Warren et al. (1998) completed

a comprehensive analysis on the profiles of the higher H Lyman series lines (from Ly-β to Ly$-\lambda$ ($n = 2, ..., 11$)). They found that: (1) the average profiles for Ly-β through Ly$-\epsilon$ ($n = 5$) are self-reversed, and the remaining lines are flat-topped; (2) the network profiles show a strong enhancement in the red wings, while the internetwork profiles are nearly symmetric; (3) the limb brightening is weak. Higher Lyman lines obtained near the limb were analysed by Marsch et al. (1999) and Marsch et al. (2000). These authors found that the line width of the Lyman lines increases with decreasing main quantum number. Schmieder et al. (1999) and Heinzel et al. (2001) presented a nearly simultaneous observation of all the hydrogen Lyman lines including the Ly-α line recorded on the attenuator of SUMER. However, the line profile was distorted by the already mentioned problem of the attenuator.

Several attempts were then made to observe Ly-α on the bare part of the SUMER detector (Teriaca et al. 2005a,b, 2006). These authors extrapolated the gain-depression correction to the high photon input rate attained during those exposures, which introduced a high uncertainty in the signal determination. Using the scattered light from the primary mirror, Lemaire et al. (1998) deduced a nearly symmetric Ly-α profile of the full-Sun irradiance. Later, Lemaire et al. (2002) compared the profiles of Ly-α and Ly-β and reported calibrated irradiances with 10% uncertainty. The relationship between the Ly-α line center irradiance and the total line irradiance was also studied by using this kind of observation (Lemaire et al. 2005; Emerich et al. 2005).

Xia (2003) studied the difference of Ly-β profiles in the coronal hole and in the quiet Sun. He found that the asymmetry of the average Ly-β line profile – the red-horn dominance – is stronger in the quiet Sun than in the coronal hole. He also found more locations with blue-horn dominance in Ly-β profiles in coronal holes than in quiet-Sun regions. By fitting the two wings of the Ly-β profiles, Xia et al. (2004) derived the Doppler shift of the line, which was found to have a correlation with the Doppler shift of the typical transition region lines C II and O VI.

Hydrogen Lyman lines were frequently used to reveal information on the fine structures and physical properties of quiescent solar prominence. Since different Lyman lines and their line center, peak, and wings are formed at different depths within the prominence thread, the Lyman series are important to diagnose the variation of the thermodynamic conditions from the prominence-corona transition region (PCTR) to the central cool parts (Vial et al. 2007). To explain the properties of observed Lyman line profiles, multi-thread prominence fine-structure models consisting of 2D threads with randomly assigned line-of-sight (LOS) velocities were developed (Gunár et al. 2008). With the assumption of magnetohydrostatic (MHS) equilibrium, the models are based on an empirical PCTR and use calculations of non-LTE (local thermodynamic equilibrium) radiative transfer. Such models have shown that the profiles of Lyman lines higher than Ly-α are more reversed when seen across than along the magnetic field lines (Heinzel et al. 2005). This behaviour was confirmed in a prominence observation by Schmieder et al. (2007).

A recent study showed that a LOS velocity of the order of 10 km/s can lead to substantial asymmetries of the synthetic line profiles obtained by the multi-thread modelling (Gunár et al. 2008). This work also predicted that the Ly-α profiles may exhibit an asymmetry opposite to those of higher Lyman lines. The ratio of Ly-α/Ly-β is also very sensitive to the physical and geometrical properties of the fine structures in prominences, and the fluctuations of this ratio are believed to relate to such fine structures (Vial et al. 2007). The *OSO* 8 observation yielded a

value of 65 (in the energy unit) for this ratio (Vial 1982), while a recent SUMER observation revealed a different ratio (96, 183, and 181, in the energy unit) in different parts of a prominence (Vial et al. 2007).

The Ly-α and Ly-β line profiles can also be used to diagnose nonthermal effects in solar flares, e.g. the nonthermal ionization of hydrogen by electron beams. It is predicted that, at the early stage of the impulsive phase of flares, the nonthermal effect should be strong and the Ly-α and Ly-β profiles will be broadened and enhanced, especially in their wings; and after the maximum of the impulsive phase, the intensity will decrease rapidly due to a rapid increase of the coronal column mass (Hénoux et al. 1995; Fang et al. 1995).

The Lyman line profiles observed in sunspot regions appear to be different from those in the quiet Sun. Observations have shown that the self-reversals are almost absent in sunspot regions (Fontenla et al. 1988; Curdt et al. 2001; Tian et al. 2009). In contrast, the lower Lyman line profiles observed in the plage region are obviously reversed, a phenomenon also found in the normal quiet Sun (Tian et al. 2009). These results indicate a much smaller opacity above sunspots, as compared to the surrounding plage region.

It was proposed that the asymmetries of the Lyman lines are probably related to large-scale motions of the atmosphere (Gouttebroze et al. 1978). In the energy-balance model of the chromosphere-corona transition region (Fontenla et al. 2002), the authors concluded that the H and He line profiles are greatly affected by flows, while in a recent multi-thread prominence model it was suggested that asymmetrical line profiles are produced by the combined effects of different Doppler shifts and absorption coefficients (optical thicknesses) in the individual threads (Gunár et al. 2008). The authors also suggested that opposite asymmetries in the profiles of Ly-α and higher Lyman lines are probably caused by different line opacities. However, much further work is still needed to understand the origin of the line asymmetries.

In a previous paper (Curdt et al. 2008b), we presented results of a non-routine observation sequence, in which we partly closed the aperture door of SUMER to reduce the incoming photon flux to a 20%-level and obtained high spectral and spatial resolution profiles of Ly-α and Ly-β. We have shown that the averaged profiles of Ly-α and Ly-β exhibit opposite asymmetries, and that the asymmetries depend on the Doppler flows in the transition region. However, in that observation, the profiles of Ly-α and Ly-β were obtained in a sit-and-stare mode, and thus only a small vertical slice of the Sun was sampled.

In this paper, we will present results of a more recent observation, in which we scanned a rectangular region around the quiet Sun disk center and obtained profiles of Ly-α and Ly-β quasi-simultaneously. This is a unique data set, since such an observation was never carried out before. We find that the spatial distribution of profiles with different self-reversals is correlated with the network pattern, and that the dependence of the profile asymmetries on the transition-region Doppler flows is different for Ly-α and Ly-β.

2. Observation and data reduction

Motivated by the results obtained recently from a sit-and-stare observation (for details cf., Curdt et al. 2008b), we modified the observing sequence and rastered a rectangular region near the solar disk center in order to get a better selection of solar features
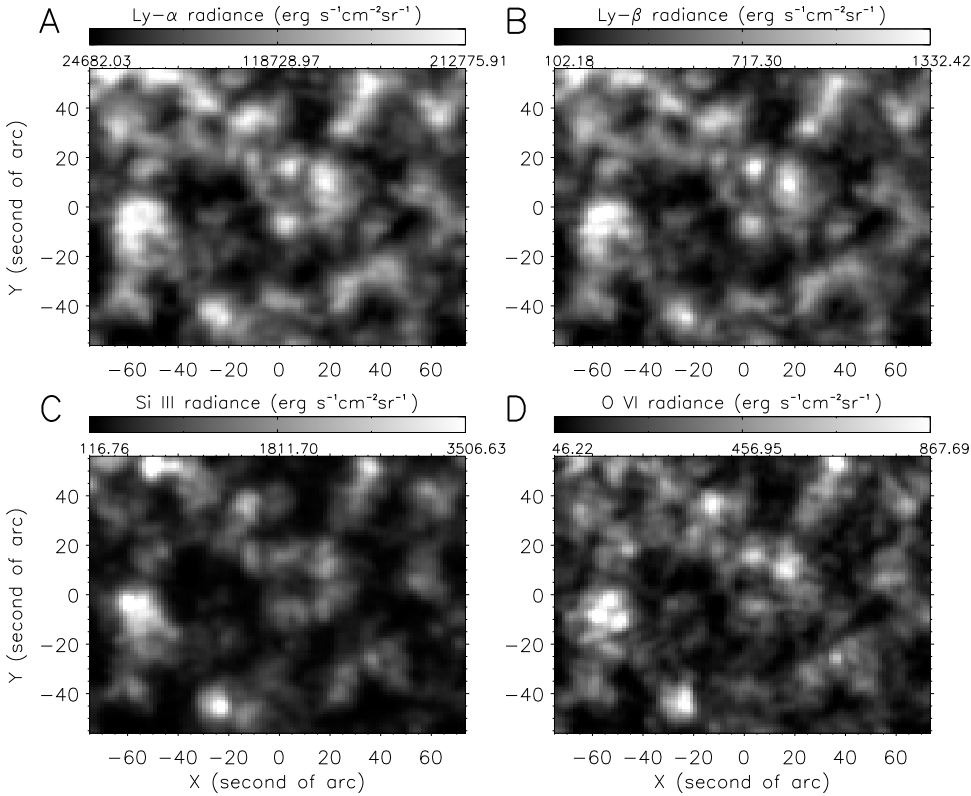
Fig. 1. Radiance maps of two Lyman and two transition-region lines: (A) Ly-α ($\lambda\,1216$), (B) Ly-β ($\lambda\,1025$), (C) Si III ($\lambda\,1206$), and (D) O VI ($\lambda\,1032$).

in the data set. The high quality of this observation allows the detailed statistical analysis presented here.

The SUMER observation was made at the central part of the solar disk from 21:59 to 23:18 on September 23, 2008. Similarly to the observation on July 2, 2008 (Curdt et al. 2008b), we partly closed the aperture door – during a real-time commanding session prior to the observation and re-opening thereafter – and could thus reduce the input photon rate by a factor of $\approx$5. As a prologue to the observation, full-detector images in the Lyman continuum around 880 Å were obtained with open and partially-closed door. At this wavelength setting, the illumination of the detector is rather uniform, and no saturation effects had to be considered. In this way, accurate values for the photon flux reduction could be established. We found that the incoming photon flux was reduced to a 18.3% level.

After this prologue, the slit 7 ($0.3'' \times 120''$) was used to scan a rectangular region with a size of about $150'' \times 120''$ at the disk center. We had to use this narrow slit to avoid saturation of the detector. We completed the raster with an increment of $1.5''$, a value which is comparable to the instrument point spread function (instrumental resolution), so that undersampling effects should be minor. For each spectral setting two spectral windows were transmitted to the ground. For the Ly-α setting, 100 pixels (px) around the $\lambda\,1216$ H I line were recorded on the bare photocathode of the detector, and 50 px around the $\lambda\,1206$ Si III line on the KBr part of the photocathode, respectively; for the Ly-β setting, 100 px around the $\lambda\,1025$ H I line and 50 px around the $\lambda\,1032$ O VI line, were recorded both on the KBr-coated section. With an exposure time of 15 s, all lines were recorded on detector B, with sufficient counts for a good line-profile analysis. Each time, the back-and-forth movement of the wavelength mechanism between subsequent exposures lasted for $\approx$10 s and led to a cadence of 50.5 s. The observed region on the Sun was very quiet during our observations.

The standard procedures for correcting and calibrating the SUMER data were applied, including local-gain correction, dead-time correction, flat-field correction, destretching, and radiometric calibration. To complete the flat-field correction, we used the flat-field exposure acquired on June 28, 2008. It turned out that there is a small shift of this flat field relative to the actual data. Therefore we shifted the correction matrix by a fraction of a pixel (0.3 pixel in solar-X, and 0.7 pixel in solar-Y) before completing the correction.

In order to improve the statistics, we averaged the nine profiles in a square of 3×3 pixels centered at each spatial pixel. This process is like a running average of the profiles in both spatial dimensions and will definitely increase the signal-to-noise ratio. Then the radiances of the observed spectra were divided by the factor of the photon flux reduction, which was 18.3% in this observation. The line radiance of each profile was obtained through an integration of the line profile. The calibrated radiance maps of the four lines are presented in Fig. 1.

During the SUMER observation, high-rate magnetograms were also obtained by the Michelson doppler imager (MDI, Scherrer et al. 1995) onboard SOHO. The magnetograms have a pixel size of about $0.6''$ and reveal clearly the magnetic fluxes in the network. In order to find a possible correlation between the magnetic flux and the Ly-α and Ly-β profiles, we selected nine magnetograms observed from 22:06 to 22:15 UT and averaged them to increase the signal-to-noise ratio.

3. The self-reversal of the profiles

In the normal quiet Sun region, most Ly-α and Ly-β line profiles exhibit a self-reversal at their centers (Warren et al. 1998; Curdt et al. 2008b). The depth of the self-reversal is a measure of the degree to which the Lyman line emission is absorbed by the hydrogen atoms in upper layers.
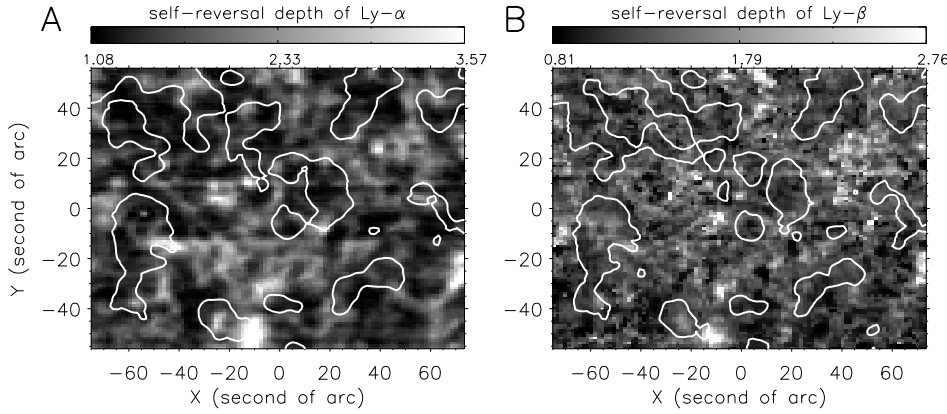
Fig. 2. Maps of the self-reversal depth (represented by R_{br2c}) of the Ly-α and Ly-β line profiles, respectively. The white contours (enclosing the top 25% values) represent the brightest parts on the corresponding radiance maps A and B of Fig. 1.
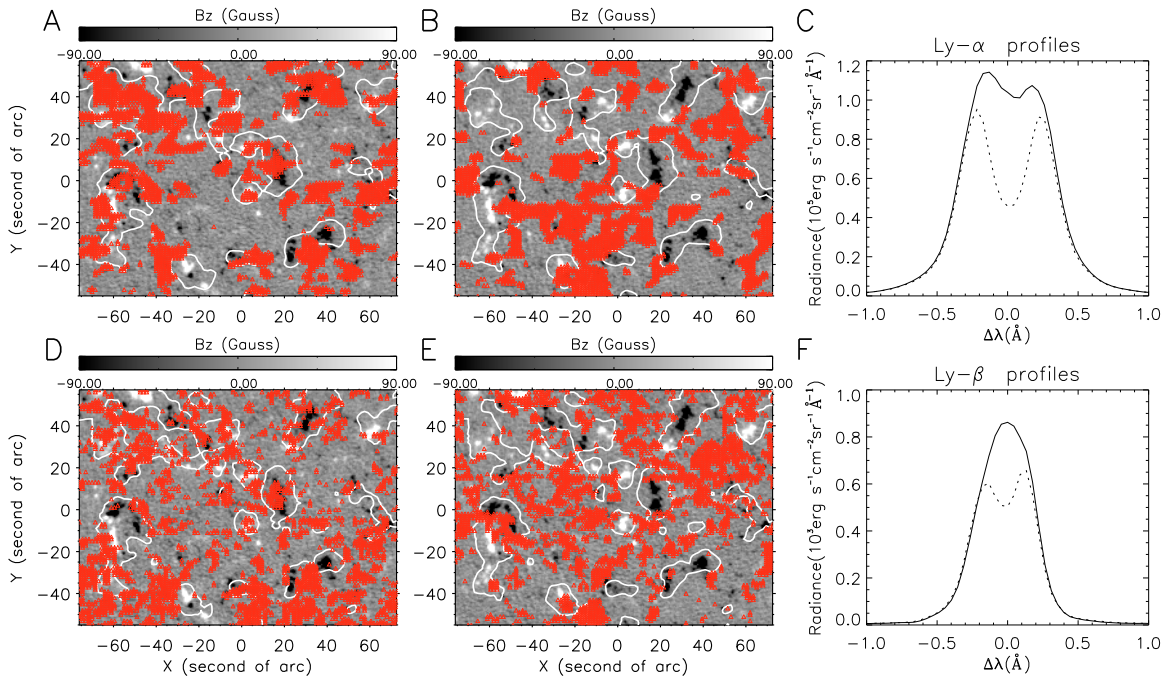

Fig. 3. Positions of Ly-α (*upper panels* A and B) and Ly-β (*lower panels* D and E) profiles having shallow (*left panels*, corresponding to the 25% smallest values of R_{br2c}) or deep (*central panels*, corresponding to the 25% largest values of R_{br2c}) self-reversals. The locations are marked by red triangles on the grey-scale MDI magnetogram. The white contours (enclosing the top 25% values) represent the brightest part on the corresponding radiance map. The averaged Ly-α profiles at positions marked in panel A/B are shown as the solid/dotted line in panel C. And the averaged Ly-β profiles at positions marked in panel D/E are shown as the solid/dotted line in panel F.

We first measured the maximum spectral radiances of the two horns (the selected spectral range is 0.12 Å–0.35 Å from the line center for Ly-α and 0.09 Å–0.24 Å from the line center for Ly-β) and the minimum spectral radiance of the central part (within 0.12 Å from the line center for Ly-α and 0.09 Å from the line center for Ly-β). The resulting spectral radiances of the central part, blue and red horns are designated by I_c, I_b and I_r, respectively. By comparing the horn radiances with the central radiance, we find that almost all of the Ly-α profiles are obviously self-reversed (only 3 profiles are flat-topped), while about 17% of the Ly-β profiles are flat-topped or not reversed. For the non-reversed profiles, I_c was calculated as the mean value of the spectral radiance of the central part, instead of the minimum value. The extent of the self-reversal is an indicator of the opacity and can be quantified by the ratio of the average horn intensity relative to the central intensity, which is designated by $R_{br2c} = 0.5(I_b + I_r)/I_c$. Although this method might not be very accurate for some profiles which are too noisy or

have no obvious central reversal and horns, in a statistical sense the parameter R_{br2c} should be a good candidate to represent the relative depth of the self-reversal of different profiles. After calculating the value of R_{br2c} for each profile, we constructed maps of the self-reversal depths of Ly-α and Ly-β as shown in Fig. 2. The white contours (enclosing the top 25% values) on the maps represent the brightest parts on the corresponding radiance maps of Fig. 1, which clearly outline the network pattern.

The self-reversal depths of both Ly-α and Ly-β profiles shown in Fig. 2 are statistically smaller in the network than in the internetwork, which indicates that the internetwork emissions are subject to stronger absorption than those in the network. This behaviour is confirmed in Fig. 3, in which the positions of weakly (corresponding to the 25% smallest values of R_{br2c}) or strongly (corresponding to the 25% largest values of R_{br2c}) absorbed emissions are marked with red triangles. The background image is an MDI magnetogram, and the contours are the same as those in Fig. 2. The averaged profiles with shallow and deep
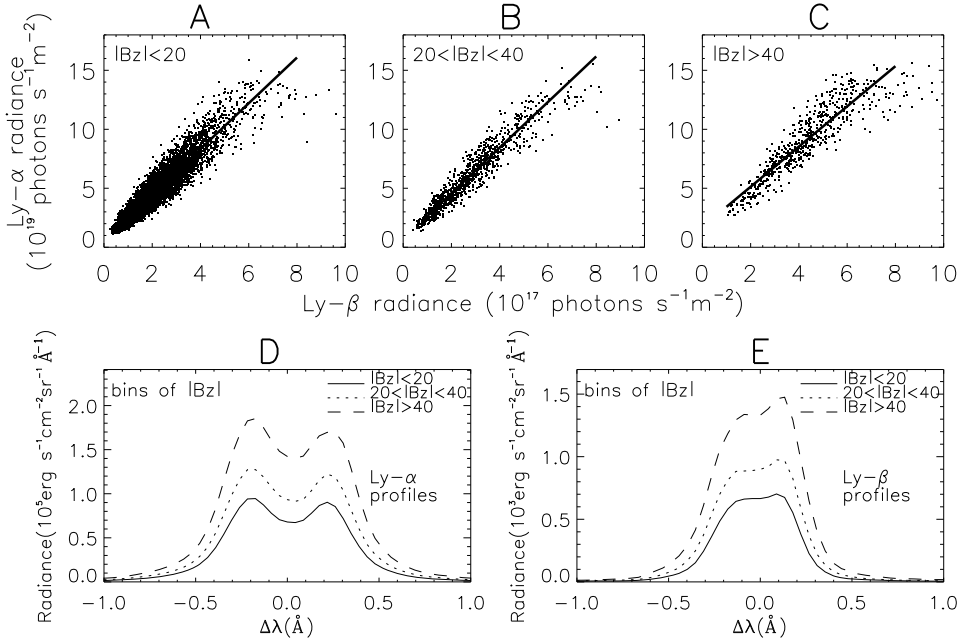
reversals are presented in the right panels, which clearly reveals the difference. From Figs. 3A and D we find that the locations of some weakly absorbed emissions deviate a little bit from the network lanes, which might be the result of the expansion of the magnetic structures in the network, since the absorption is mainly occurring at higher layers (upper chromosphere and TR). We have to mention that the above result is only a statistical correlation, since some weakly and strongly absorbed emissions are still found at internetwork and network locations, respectively. And one has to bear in mind that the effect of profile asymmetry can not be excluded in the calculation of the ratio R_{br2c}. For instance, this ratio will have a similar value for, e.g., a symmetric profile with two horns of equal radiance, and an asymmetric profile with a stronger horn on one side and a weaker horn on the other side. But it is not straightforward to say if they are equally reversed. Also, our method may not be appropriate for some noisy profiles and some profiles without obvious central dips. This effect can be neglected for Ly-α, but it has an impact on the results for Ly-β because of its weaker emission and absorption. However, by checking individual profiles, we confirmed the correlation shown in Fig. 3.

Our result that the Lyman line emissions are more strongly absorbed in the internetwork as compared to the network seems to be related with the different magnetic structures in the two regions. There is no doubt that most of the Ly-α and Ly-β emissions come from the chromosphere and lower TR (Fontenla et al. 1988). Network is the location where magnetic flux converges, and from which magnetic funnels (which might be related to solar wind, or just be the legs of trans-network loops) originate (Peter 2001). In the network, loops of different sizes and funnels are crowded in the chromosphere and transition region, and the Lyman line emissions originate from the outskirts of these magnetic structures. However, in the internetwork region, only low-lying loops are present and most of the Lyman line emission sources are located at a much lower height as compared to the network. This scenario leads to an enhanced opacity in the internetwork and thus the Lyman radiation penetrating the upper layers will be more strongly absorbed in the internetwork than the network.

However, we should mention that possible differences of the density and temperature gradient in the two regions might also play a role in the process of absorption. We should not exclude these possibilities. To fully understand our observational result, new detailed atmospheric models and radiative transfer calculations will by required.

Our radiance data also allow us to test the relationship between the central Ly-α spectral radiance and the total Ly-α line radiance published by Emerich et al. (2005). The resulting scatter plots (not shown here) suggest an almost linear relationship and a ratio of the central spectral radiance to full line radiance of 9.43 ± 0.04. Our value is lower than the *OSO*-5 result (Vidal-Madjar 1975), and in closer agreement with the previous irradiance results of Emerich et al. (2005) and Lemaire et al. (2005).

4. Ratio between Ly-α and Ly-β intensities

One advantage of this observation over the last one is that we have simultaneous high-rate MDI magnetograms. Thus we can sort all the profiles according to the absolute values of the vertical magnetic field strength, $|B_z|$, in order to find whether there is a relationship between the magnetic field and the profile asymmetry. We defined two thresholds, 20 Gauss and 40 Gauss, and averaged the profiles of Ly-α and Ly-β in three bins. The results are presented in Fig. 4. A scatter plot of the relationship between the Ly-α and Ly-β radiances in each bin is also presented in that figure.

In our previous study (Curdt et al. 2008b), we reported that the average radiances of the two lines yield a Ly-α/Ly-β photon ratio of ≈188. This result was surprising, since it significantly deviates from values reported by Vial (1982) and Vernazza & Reeves (1978). Here, again we applied a linear fit to a scatter plot, and found values very similar to those obtained in the sit-and-stare study. For three different magnetic field bins (with increasing magnetic field strength) we found photon ratios of 193.6 ± 0.8, 193.1 ± 2.0, and 170.3 ± 3.2, respectively. However, from Fig. 4 we can infer that some dots with high radiances significantly deviate from the fitting line, which indicates

Table 1. The observed ratios between Ly-α and Ly-β photon radiances.

Reference	Target	Ratio	Instrument
Vernazza & Reeves (1978)	quiet Sun	102	ATM UV Spectrometer
Vernazza & Reeves (1978)	coronal hole	108	ATM UV Spectrometer
Vernazza & Reeves (1978)	active region	42	ATM UV Spectrometer
Lemaire et al. (1978)	full Sun	79	LPSP/OSO 8
Vial (1982)	prominence	77	LPSP/OSO 8
Lemaire et al. (2005)	full Sun	155	SUMER/SOHO
Vial et al. (2007)	prominence	114-217	SUMER/SOHO
Curdt et al. (2008b)	quiet Sun	188	SUMER/SOHO
Current paper	quiet Sun	212-230	SUMER/SOHO

that the ratio should be smaller in very bright-emission regions. We calculated the median value of the ratio of Ly-α/Ly-β, and found that the ratio is 229.575, 222.805 and 212.737 in the three bins. It seems that there is a weak declining trend of the line ratio with increasing magnetic field strength. However, the deviation in regions with very bright emission could also be due to unidentified saturation effect in the detection system. Thus the insignificant difference among the three values seems to suggest that the ratio of Ly-α and Ly-β intensities is independent of magnetic field strength.

Recently, and also based on a SUMER observation, Vial et al. (2007) obtained varying Ly-α/Ly-β radiance (in the energy unit) ratios of 96, 183, and 181 in different parts of a prominence. They were explained as relating to the fine structures in prominences. In view of the high quality of our new data set, we are now confident that these high values of the photon ratio are reliable within an estimated 10% uncertainty. Table 1 lists the observed ratios between Ly-α and Ly-β photon radiances. Some previous results using energy units have been converted into photon units, by multiplying a factor of 1216/1025.

5. Asymmetry of the profiles

Figures 4D and E reveal clearly that the profile asymmetry has a dependence on the magnetic field strength, and the asymmetries of the average Ly-α and Ly-β profiles are opposite. Curdt et al. (2008b) found that the blue-horn asymmetry of Ly-α and red-horn asymmetry of Ly-β tend to be more prominent at locations where significant downflows are present in the transition region. Our result is consistent with the Dopplershift-to-asymmetry relationship in Curdt et al. (2008b), since larger red shift is usually found in the magnetic network. Thus we have confirmed that the averaged profile is stronger in the blue horn for Ly-α, and stronger in the red horn for Ly-β.

In our previous paper (Curdt et al. 2008b), we found that there is a relationship between the profile asymmetry and the Doppler shift in the TR. We also found that the averaged profiles of Ly-α and Ly-β have opposite asymmetries. However, in the observation on July 2 of 2008, SUMER was operated in sit and stare mode so that only spectra emitted from a narrow slice of the Sun were recorded. In the current observation, we scanned a region which included several network cells. We calculated the Doppler shifts of Si III and O VI by applying a single Gaussian fitting to the corresponding line profiles. Using a similar analysis method, we confirmed that the Dopplershift-to-asymmetry relationship also exists in this new data set. Since the results are basically the same, there is no need to present them here.

We have to mention that there is no strict (pixel-to-pixel) correlation between the blue-horn asymmetry in Ly-α and red-horn asymmetry in Ly-β. At some locations the Ly-α and Ly-β profiles have the same sign of asymmetry, but may have

opposite signs of asymmetry at other locations. This finding seems to indicate that different processes may be responsible in both cases and is consistent with the prediction of a recent prominence model (Gunár et al. 2008), in which the authors included both effects of Doppler shift and opacity to calculate synthetic line profiles. We also find that most Ly-α profiles are stronger in the blue horn, while most Ly-β profiles are stronger in the red horn.

To study the asymmetry of the Lyman line profiles quantitatively, we calculated the 1st and 3rd order moments of the profiles.

5.1. Moments of the line profiles

The calculation of the moments of a Lyman line profile allows one to characterize it quantitatively and to determine numbers for its relative shift, asymmetry, peakness, and so on. Thus, one can obtain valuable information on the state and dynamics of the solar atmosphere. Following the definition of Gustafsson et al. (2006), we computed the following brightness-weighted statistical moments:

$$\text{mean wavelength: } \lambda_c = \frac{\sum (I_i - B_i)\lambda_i}{\sum (I_i - B_i)}, \quad (1)$$

$$\text{standard deviation: } \sigma = \sqrt{\frac{\sum (I_i - B_i)(\lambda_i - \lambda_c)^2}{\sum (I_i - B_i)}}, \quad (2)$$

$$\text{skewness: } \frac{\sum (I_i - B_i)(\lambda_i - \lambda_c)^3}{\sigma^3 \sum (I_i - B_i)}, \quad (3)$$

where I_i, B_i, and λ_i represent, respectively, the spectral radiance, background, and wavelength (here in the unit of a spectral pixel i, which is about 42 mÅ). For the sake of simplicity, we assumed a constant continuum background, with the level being given by the lowest spectral radiance of the profile. After calculating the moments for each profile, we constructed a map of each moment of Ly-α and Ly-β. Here we only present the maps of the 1st and 3rd order moments of the two Lyman lines in Fig. 5. The white contours (enclosing the top 25% values) on the maps represent the brightest parts on the corresponding radiance map of Fig. 1, which clearly outline the network pattern.

The 1st-order moment represents the mean spectral position of the profile. Since we are mainly interested in the relative position, we subtracted the average (over the entire studied region) mean position from the mean position of each profile. The resulting value will be referred to as the 1st-order moment in our later discussion. It corresponds to the Doppler shift in the case of a Gaussian-shaped profile. However, in the case of Ly-α and Ly-β, not only the Doppler shift of the line, but also the asymmetry of the line profile can contribute to the 1st-order moment.
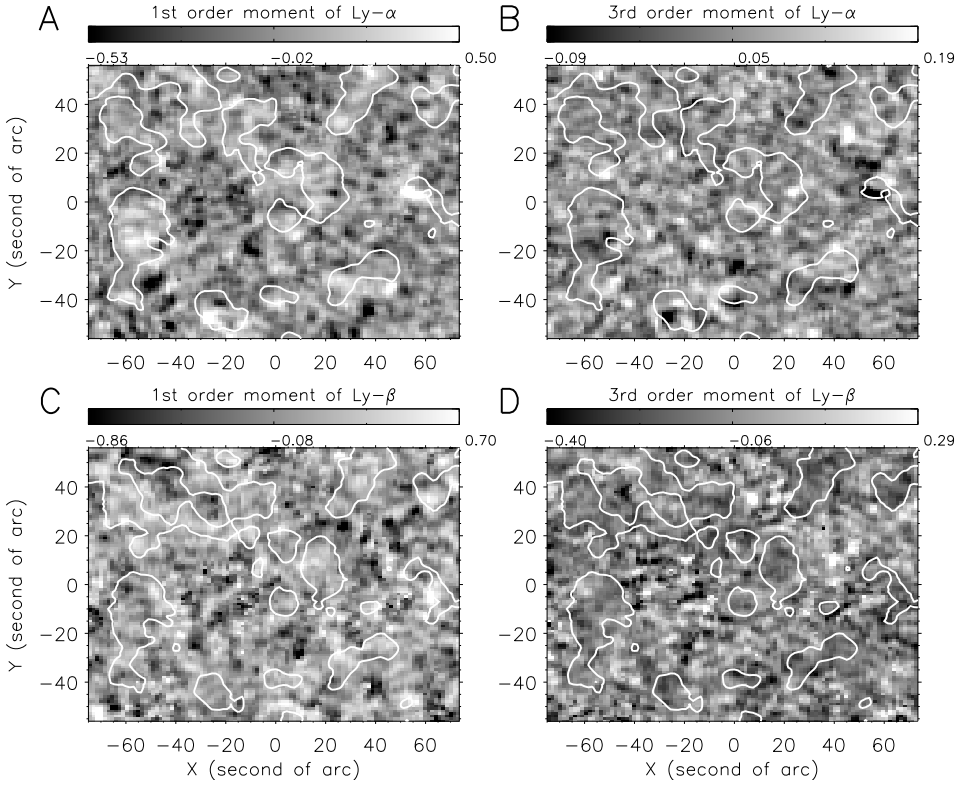
The 2nd-order moment is the standard deviation of the profile. In the case of Ly-α and Ly-β, it includes information on both the line width and the self-reversal depth. However, a narrow profile with a deep self-reversal and a broad profile with a shallow self-reversal may have a comparable value of the 2nd-order moment. Since we wanted to avoid putting these two different kinds of profiles into the same category, we did not analyse this moment in our study.

The 3rd-order moment, the skewness, is a measure of the asymmetry of the line profiles. This parameter seems to be a good candidate to study the asymmetry of Ly-α and Ly-β profiles. However, both Ly-α and Ly-β are blended with a He II line in the blue wing. This blend will definitely influence the calculation of the 3rd-order moments. The problem for Ly-β is even worse, since the line is much narrower and weaker than Ly-α so that the He II blend contributes more to the skewness of Ly-β. And even more, there is another O I blend in the central part of the Ly-β profile. The mixture effect of the blends can be seen in the values calculated from Eq. (3). Therefore, these values were adjusted by adding 0.05 for Ly-α and subtracting 0.24 for Ly-β, to make those profiles with equal-height horns correspond to a zero value of skewness.

We have sorted the profiles by each moment and defined six bins which were equally spaced in the moment. The average profiles in each bin are shown in Fig. 6. Again, only the results of the 1st and 3rd order moments, which we are mainly interested in, are presented. The averaged profiles exhibit obvious signatures of asymmetry, which will be further investigated in the next two sections.

5.2. Discussion

It is not easy to find a parameter which can purely reflect the asymmetry of the Lyman line profiles. However, from Fig. 6 the 1st- and 3rd-order moments seem to reveal some information,

although not purely, on the line asymmetry. As mentioned previously, both the shift of the entire profile and the asymmetry of the profile can contribute to the 1st-order moment of Ly-α and Ly-β. A red-shifted profile with a stronger red wing will definitely lead to a larger value of the 1st-order moment. In contrast, a blue-shifted profile with a stronger blue wing should correspond to a smaller value of the 1st-order moment. From panels A and C of Fig. 5 we find that in statistical sense, both Ly-α and Ly-β have a larger value of their 1st-order moment in the network than in the internetwork. This behaviour indicates that the average network-related profile is either largely red-shifted or strongly enhanced in the red wing. As mentioned previously, the 3rd-order moment, i.e., the skewness of the Ly-α and Ly-β profile, is influenced by the blends. However, by inspection of Fig. 6 we find that the asymmetries of the Lyman line profiles still can somehow be reflected in the values of the 3rd-order moment. A negative/positive value of this parameter corresponds to a profile with an enhanced red/blue horn.

Since the asymmetries of the Lyman line profiles are caused by a combined effect of Doppler shift and opacity (Gunár et al. 2008), we may find that there is a relationship between the 1st and 3rd order moments and the Doppler shift. Here we can only calculate the Doppler shifts of two transition region lines, Si III and O VI. In Fig. 7, we present the dependence of the 1st and 3rd order moments of Ly-α and Ly-β on the Doppler shifts of Si III and O VI.

It is clear that the 1st-order moment of Ly-β is positively correlated with the Doppler shift in the TR. This relationship is corroborated by Fig. 8, in which locations of Ly-β profiles corresponding to the 25% smallest values (upper panels) and 25% largest values (lower panels) of the 1st-order moment are marked by red triangles on the Dopplergrams of Si III/ O VI. The white contours outline the network pattern as seen on the Ly-β radiance map. This strong correlation can be understood if we assume that the Ly-β profile is more redshifted and more enhanced in the red
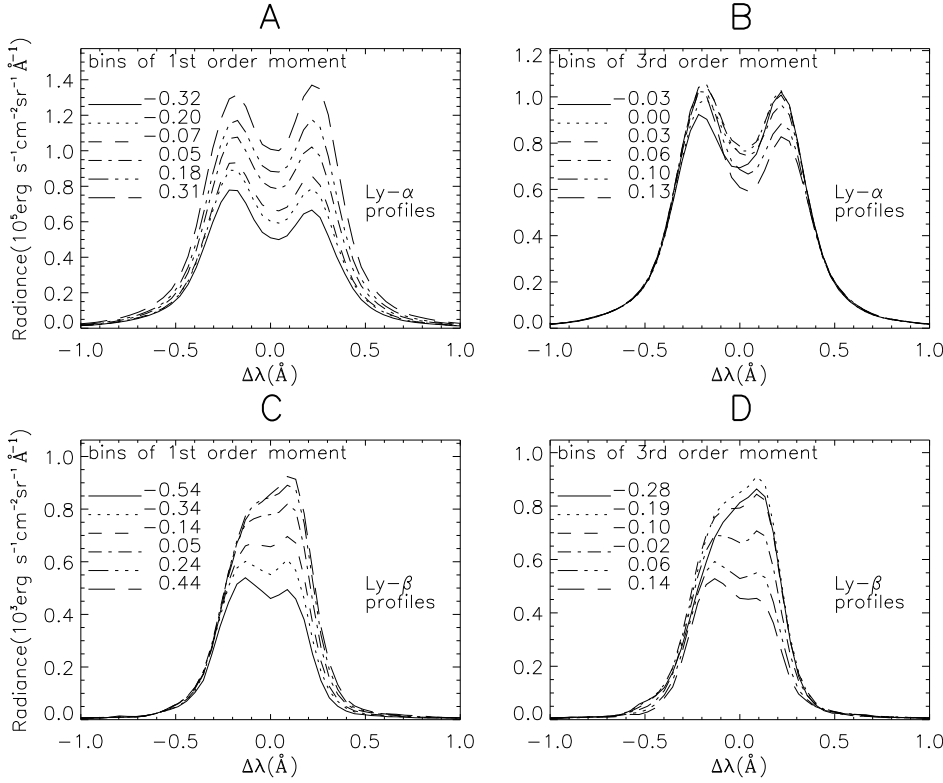
Fig. 6. Various averaged Ly-α (*upper panels* A and B) and Ly-β (*lower panels* C and D) profiles in bins of each moment. The level of each bin is also shown in the plots, and the corresponding profiles are represented by different line styles.
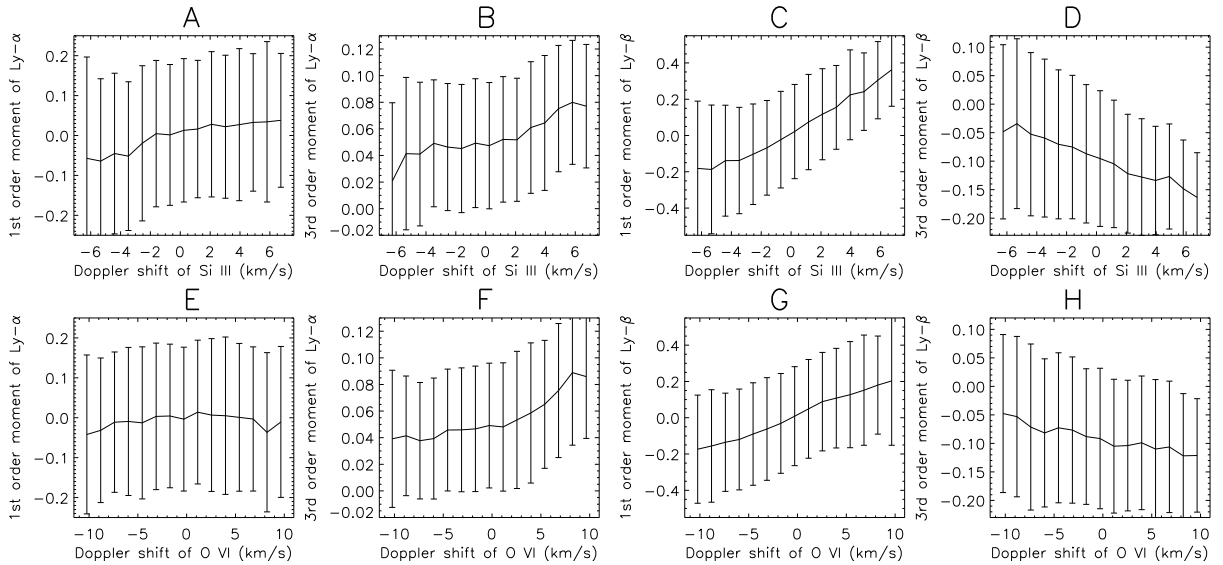

Fig. 7. Dependence of the 1st and 3rd-order moments on the Doppler shifts of the Si III line (panels A to D) and O VI line (panels E to H). A positive and negative value of the Doppler shift indicates redshift (downflow) and blueshift (upflow), respectively. The error bar indicates the standard deviation of the corresponding moment in each bin.

horn in regions where larger TR downflows are present. Panels D and H of Fig. 7 reveal a clear decreasing trend of the skewness with increasing TR Doppler shift, which means that the red horn of Ly-β tends to be more enhanced where the Doppler shift is larger.

To further substantiate this result, we extended the analysis on the data set used for the spectral atlas of Curdt et al. (2001) and completed a detailed wavelength calibration for Ly-β, based on nearby fluorecence lines of neutral oxygen as wavelength standards. These lines are radiatively excited, probably by Lyman continuum photons via the 3s, 3d, and 4s levels of the O I triplet system. We assume that these optically thin O I lines

emerge from the lower chromosphere (Avrett & Loeser 2008) and are at rest, at least within the required uncertainties. We could reproduce the average line profile with a multigauss fit of a broad Gaussian line (≈0.3 A *FWHM*) with a redshift of 5 km s^{-1}, the He II Balmer line in the blue wing, a much narrower Gaussian absorption profile (≈0.15 A *FWHM*), and the O I lines as wavelength standards. Because of the lack of wavelength standards and the much stronger absorption, this method cannot be used for Ly-α.

This redshift of 5 km/s is comparable to the average redshift of a typical TR line (Brekke et al. 1997; Warren et al. 1997; Chae et al. 1998; Xia 2003). In addition, following the method
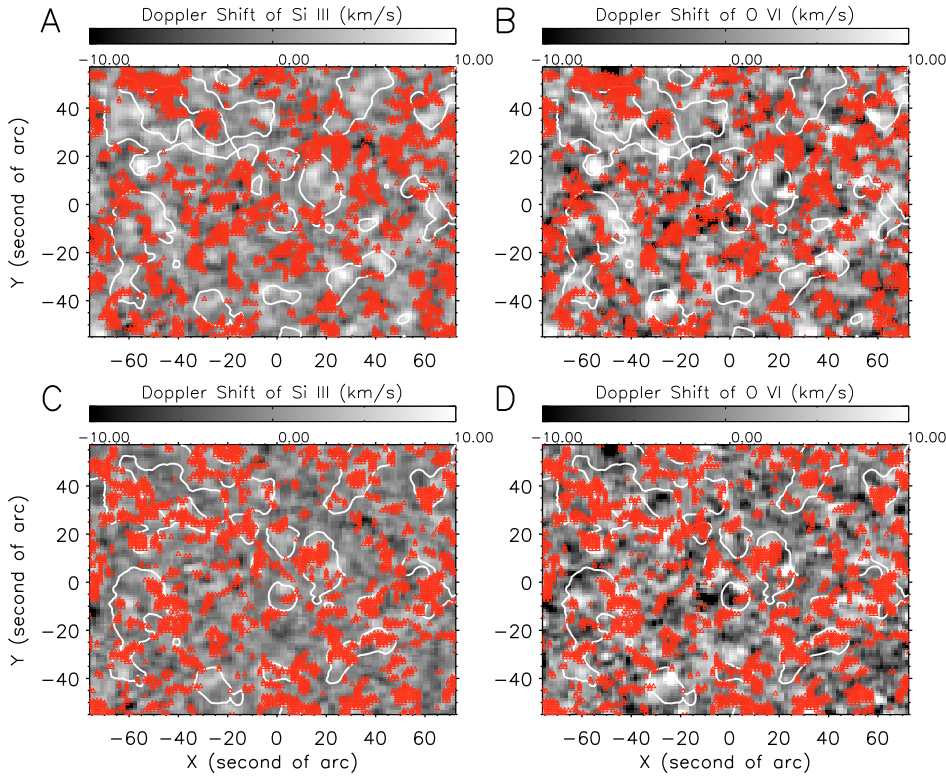
Fig. 8. Locations of the Ly-β profiles corresponding to the 25% smallest values (*upper panels*, A and B) and the 25% largest values (*lower panels*, C and D) of the 1st-order moment, which are marked by small red triangles on the grey-shaded Dopplergrams of the Si III and O VI lines. The white contours (enclosing the top 25% of the radiance values) represent the brightest parts on the Ly-β radiance map.

described in Curdt et al. (2008a), we divided the average network profile by the average internetwork profile and obtained the network contrast profile for Ly-β (not shown here). We found that there is a clear peak of this network contrast profile on the red side of the line profile, which indicates that the Ly-β line is redshifted. Such a behaviour is similar to typical TR lines and a natural result of the well-known brightness-Doppler-shift relationship. Although the hydrogen Lyman lines are mainly formed in the chromosphere and lower TR, since hydrogen is the most abundant element in the solar atmosphere, there should still be some emission sources of its resonance lines in the middle and upper TR. Ly-β is optically thinner than Ly-α, and we can see substantial Ly-β emission from the TR. That is why the behaviour of Ly-β is similar to typical TR lines.

Panels B and F of Fig. 7 reveal a clear increasing trend of the skewness with increasing TR Doppler shift, which means that the blue horn of Ly-α tends to be more enhanced if the TR redshift is larger. This is consistent with the result of Curdt et al. (2008b). From panels A and E of Fig. 7 we find that the 1st-order moment of Ly-α tends to slightly increase or stay the same with increasing TR Doppler shift. As we mentioned previously, both the Doppler shift of the whole profile and the profile asymmetry can contribute to the 1st-order moment. Since the enhanced blue horn will reduce the moment, the only possibility is that Ly-α is more redshifted in regions where larger downflows are present.

The large scatters in Fig. 7 suggest that besides the TR flows, there should be other effects which can influence the asymmetry of the Lyman line profiles. We have to mention that the explanation of the asymmetries of the Ly-α and Ly-β profiles will require intricate modelling rather than simple imagination. Their different asymmetries arise from the motions of the solar atmosphere in its different layers as well as from the different line opacities. Further theoretical work, especially modelling, is needed to improve our understanding of the formation of the Lyman line profiles.

As mentioned above, energy losses through the Ly-α emission are the most important radiative losses in the lower TR (Fontenla et al. 1988). Thus the Ly-α line should be important for the diagnostic of the magnetic and plasma properties in the lower TR. It is still under debate if the TR emission originates from a thin thermal interface connecting the chromosphere and corona (Gabriel 1976; Dowdy et al. 1986; Peter 2001), or from isolated unresolved tiny loops (Feldman 1983, 1987; Feldman & Laming 1994). Recently, Patsourakos et al. (2007) reported the first spatially resolved observations of subarcsecond-scale (0.3″) loop-like structures seen in the Ly-α line, as observed by the Very High Angular Resolution Ultraviolet Telescope (VAULT). As mentioned in that paper, flows can have distinct spectroscopic signatures, which can help to distinguish between the two possibilities of the TR emission origin. However, the signature of flows in the corona is missing in the SUMER observation. Moreover, the spatial resolution of our SUMER observation is still not high enough. Thus we can still not make a final conclusion on the origin of the TR emission. We think that only through a combined analysis of high-resolution (subarcsecond) magnetic field, EUV imaging, and spectroscopic observations can further substantial progress be expected.

6. Summary and conclusion

We have presented new results from a quasi-simultaneous observation of the profiles of Ly-α and Ly-β. We find that the self-absorption in or around network is reduced, and in the internetwork region the emissions tend to be more strongly absorbed in the central part of the profiles. We suggest that the different magnetic structures in the two regions might be responsible for this result. The outskirts of the chromospheric and transition-region magnetic structures, where the Lyman line emissions originate, are higher in the network as compared to the internetwork.

Using the simultaneously measured photospheric magnetic field, we could determine the ratio of Ly-α and Ly-β intensities

for different bins of magnetic field strength. Our result seems to suggest that the ratio is independent of the magnetic field strength.

A rough inspection of the line profiles suggests that most Ly-α profiles are stronger in their blue horn, while most Ly-β profiles are stronger in their red horn. But the opposite asymmetries of Ly-α and Ly-β are not strictly (on a pixel-to-pixel level) correlated.

The skewness of the profiles reveals clearly that the Ly-α and Ly-β profiles are more enhanced in the blue and red horns, respectively, if larger TR downflows are present. The first-order moment of Ly-β is strongly correlated with the Doppler shift of Si III and O VI. This result can be understood if the profiles are more redshifted in regions where larger TR downflows are present. The correlation is much weaker for Ly-α, which indicates that the Ly-α profiles should also be more redshifted if larger TR downflows are present. Through a multi-Gauss decomposition of Ly-β, we found that Ly-β is redshifted on average.

The opposite asymmetries of the average profiles of Ly-α and Ly-β are presumably caused by the combined effects of flows in various layers of the solar atmosphere and opacity difference of the two lines. A mechanism for line formation can not be simply imagined but must be thoroughly devised and further investigated by help of models.

References

Avrett, E. H., & Loeser, R. 2008, ApJS, 175, 229
Basri, G. S., Linsky, J. L., Bartoe, J.-D. F., Brueckner, G., & Van Hoosier. M. E. 1979, ApJ, 230, 924
Brekke, P., Hassler, D. M., & Wilhelm, K. 1997, Sol. Phys., 175, 349
Chae, J., Schühle, U., & Lemaire, P. 1998, ApJ, 505, 957
Curdt, W., Brekke, P., Feldman, U., et al. 2001, A&A, 375, 591
Curdt, W., Tian, H., Dwivedi, B. N., & Marsch, E. 2008a, A&A, 491, L13
Curdt, W., Tian, H., Teriaca, L., Schühle, U., & Lemaire, P. 2008b, A&A, 492, L9
Dowdy, J. F., Jr., Rabin, D., & Moore, R. L. 1986, Sol. Phys., 105, 35
Feldman, U. 1983, ApJ, 275, 367
Feldman, U. 1987, ApJ, 320, 426
Feldman, U., & Laming, J. M. 1994, ApJ, 434, 370
Gabriel, A. H. 1976, Philos. Trans. R. Soc. London A, 28l, 575
Emerich, C., Lemaire, P., Vial, J.-C., et al. 2005, Icarus 178, 429
Fang, C., Feautrier, N., & Hénoux, J.-C. 1995, A&A, 297, 854
Fontenla, J. M., Reichmann, E. J., & Tandberg-Hanssen, E. 1988, ApJ 329, 464
Fontenla, J. M., Avrett, E. H., & Loeser, E. 2002, ApJ, 572, 636
Gouttebroze, P., Lemaire, P., Vial, J.-C., & Artzner, G. 1978, ApJ, 225, 655
Gunár, S., Heinzel, P., Anzer,U., & Schmieder, B. 2008, A&A, 490, 307
Gustafsson, M., Field, D., Lemaire, J. L., & Pijpers, F. P. 2006, A&A, 445, 601
Heinzel, P., Schmieder, B.,Vial, J.-C., & Kotrc, P. 2001, A&A, 370, 281
Heinzel, P., Anzer, U., & Gunár, S. 2005, A&A, 442, 331
Hénoux, J.-C., Fang, C., & Gan, W.-Q. 1995, A&A, 297, 574
Lemaire, P., Charra, J., Jouchoux, A., et al. 1978, ApJ 223, L55
Lemaire P., Wilhelm K., Curdt W., et al. 1997, Sol. Phys., 170, 105
Lemaire, P., Emerich, C., Curdt, W., Schühle, U., & Wilhelm, K. 1998, A&A, 334, 1095
Lemaire, P., Emerich, C., Vial, J.-C., et al. 2002, in Proc. SOHO 11 From Solar Min to Max: Half a Solar Cycle with SOHO, ed. A. Wilson, Davos, Switzerland, ESA SP-508, 219
Lemaire, P., Emerich, C., Vial, J.-C., et al. 2005, AdSpR, 35, L384
Mariska, J. T. 1992, The Solar Transition Region (Cambridge: Cambridge Univ. Press)
Marsch, E., Tu, C.-Y., Heinzel, P., Wilhelm, K., & Curdt, W. 1999, A&A, 347, 676
Marsch, E., Tu,C.-Y., & Wilhelm, K. 2000, A&A, 359, 381
Nicolas, K. R., Kjeldseth Moe, O., & Tousey, R. 1976, JGR, 81, 3465
Patsourakos, S., Gouttebroze, P., & Vourlidas, A. 2007, ApJ, 664, 1214
Peter, H. 2001, A&A, 374, 1108
Scherrer, P. H., Bogart, R. S., Bush, R. I., et al. 1995, Sol. Phys., 162,129
Schmieder, B., Heinzel, P., Vial, J.-C., & Rudway, P. 1999, Sol. Phys., 189, 109
Schmieder, B., Gunár, S., Heinzel, P., & Anzer, U. 2007, Sol. Phys., 241, 53
Teriaca, L., Schühle, U., Solanki, S. K., Curdt, W., & Marsch, E. 2005a, in Proc. Chromospheric and Coronal Magnetic Fields, ed. D. E., Innes, A., Lagg, & S. K., Solanki (Germany: Katlenburg-Lindau), ESA SP-596, 66
Teriaca, L., Schühle, U., Solanki, S. K., Curdt, W., & Marsch, E. 2005b, in Proc. ESPM The Dynamic Sun: Challenges for Theory and Observations, ed. D., Danesy, S., Poedts, A., De Groof, & J., Andries, Leuven, Belgium, ESA SP-60, 100
Teriaca, L., Schühle, U., Solanki, S. K., Curdt, W.,& Marsch, E. 2006, in Proc. 10 years of SoHO and beyond, ed. H., Lacoste, & L., Ouwehand, Giardini-Naxos, Italy, ESA SP-617, 77
Tian, H., Curdt, W., Teriaca, L., Landi, E., & Marsch, E. 2009, A&A, [DOI:10.1051/0004-6361/200912114]
Vernazza, J. E., & Reeves, E. M. 1978, ApJS, 37, 485
Vidal-Madjar, A. 1975, Sol. Phys. 40, 69
Vial, J.-C. 1982, ApJ, 253, 330
Vial, J.-C., Ebadi, H., & Ajabshirizadeh, A. 2007, Sol. Phys., 246, 327
Warren, H. P., Mariska, J. T., Wilhelm, K., & Lemaire, P. 1997, ApJ, 484, L91
Warren, H. P., Mariska, J. T., & Wilhelm, K. 1998, ApJS, 119, 105
Wilhelm, K., Curdt, W., Marsch, E., et al., 1995, Sol. Phys., 162, 189
Wilhelm, K., Lemaire, P., Dammasch, I. E., et al., 1998, A&A, 334,685
Xia, L.-D. 2003, Ph.D. Thesis (Göttingen: Georg-August-Univ.)
Xia, L.-D., Marsch, E., & Wilhelm, K. 2004, A&A, 424, 1025